Intrusion of warm Bering/Chukchi waters onto the shelf in the western Beaufort Sea

Stephen R. Okkonen,[1] Carin J. Ashjian,[2] Robert G. Campbell,[3] Wieslaw Maslowski,[4] Jaclyn L. Clement-Kinney,[4] and Rachel Potter[1]

[1] Wind-driven changes in the path of warm Bering/Chukchi waters carried by the Alaska Coastal Current (ACC) through Barrow Canyon during late summer are described from high-resolution hydrography, acoustic Doppler current profiler–measured currents, and satellite-measured sea surface temperature imagery acquired from mid-August to mid-September 2005–2007 near Barrow, Alaska. Numerical simulations are used to provide a multidecadal context for these observational data. Four generalized wind regimes and associated circulation states are identified. When winds are from the east or east-southeast, the ACC jet tends to be relatively strong and flows adjacent to the shelf break along the southern flank of Barrow Canyon. These easterly winds drive inner shelf currents northwestward along the Alaskan Beaufort coast where they oppose significant eastward intrusions of warm water from Barrow Canyon onto the shelf. Because these easterly winds promote sea level set down over the Beaufort shelf and upwelling along the Beaufort slope, the ACC jet necessarily becomes weaker, broader, and displaced seaward from the Beaufort shelf break upon exiting Barrow Canyon. Winds from the northeast promote separation of the ACC from the southern flank of Barrow Canyon and establish an up-canyon current along the southern flank that is fed in part by waters from the western Beaufort shelf. When winds are weak or from the southwest, warm Bering/Chukchi waters from Barrow Canyon intrude onto the western Beaufort shelf.

Citation: Okkonen, S. R., C. J. Ashjian, R. G. Campbell, W. Maslowski, J. L. Clement-Kinney, and R. Potter (2009), Intrusion of warm Bering/Chukchi waters onto the shelf in the western Beaufort Sea, *J. Geophys. Res.*, *114*, C00A11, doi:10.1029/2008JC004870.

1. Introduction

[2] Warm waters of Bering Sea and Chukchi Sea origin have figured prominently in many investigations of circulation in the Chukchi and Beaufort Seas. Interest in these warm waters has greatly increased in recent years as they have been implicated in the precipitous decline of sea ice in the Arctic Ocean [e.g., *Shimada et al.*, 2006].

[3] These warm waters tend to follow the northwestern Alaskan coast in the eastern Chukchi Sea as the Alaska Coastal Current (ACC) [*Paquette and Bourke*, 1974; *Mountain et al.*, 1976]. *Hufford* [1973] identified an extensive warm water layer from widely spaced hydrographic data acquired over the slope and outer shelf in the southern Beaufort Sea that led him to infer the presence of an eastward flowing current along the Beaufort shelf break and to

suggest the source waters were from the Bering Sea. *Aagaard* [1984] identified this current as the Beaufort Undercurrent and described its mean and time-varying characteristics. *Pickart* [2004] analyzed historical current meter and hydrographic data to identify composite seasonal modes of the shelf edge circulation in the southern Beaufort, two modes of which were characterized by their Bering/Chukchi source waters: a cold, subsurface flow characteristically occurring during late spring to midsummer and a warm, surface-intensified flow typically occurring during late summer and early autumn. In the present context of diminishing Arctic sea ice, *Paquette and Bourke* [1974], who noted the interaction of the warm ACC with the ice edge in the Chukchi Sea, and *Ahlnas and Garrison* [1984], who used satellite imagery to show that sea ice was melted by this warm coastal flow, appear prescient.

[4] The aforementioned papers are only a small subset of a fairly extensive body of research on the ACC. With the possible exception of the *Hufford* [1973] paper, none explicitly focus on hydrography and circulation on the Beaufort shelf (i.e., from coastline to the shelf break) near Barrow. There is also a considerable body of research on biological and physical oceanography of the "western" Beaufort shelf. However, in this context, the western Beaufort shelf has been generalized to refer to that portion of the

[1]Institute of Marine Science, University of Alaska Fairbanks, Fairbanks, Alaska, USA.
[2]Department of Biology, Woods Hole Oceanographic Institution, Woods Hole, Massachusetts, USA.
[3]Graduate School of Oceanography, University of Rhode Island, Narragansett, Rhode Island, USA.
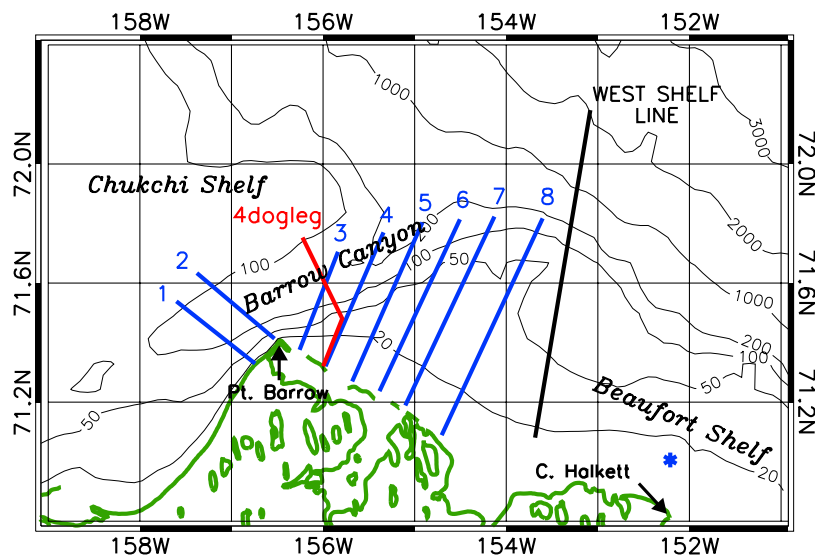[4]Department of Oceanography, Naval Postgraduate School, Monterey, California, USA.

Figure 1. Map of the Barrow study area showing hydrographic transect locations (blue) occupied in 2005–2007. Line 4 was changed to a dogleg (red) in 2007. Not all transects were occupied in each year. The asterisk denotes the location of the Cape Halkett current meter mooring. Model results are from the West Shelf Line (black).

Beaufort shelf adjacent to Alaska. Moreover, the bulk of 'western' Beaufort shelf research has been targeted on the shelf waters in the vicinity of the Prudhoe Bay oilfields. The observations (hydrography, current measurements, satellite imagery) and numerical simulations described and analyzed in the following sections were acquired in what is arguably the most poorly sampled region of the Alaskan Beaufort shelf, the westernmost portion of this shelf. These observations were acquired as components of multidisciplinary projects investigating oceanographic features and processes associated with Bowhead whale feeding hot spots near Barrow, Alaska during August–September 2005–2007.

[5] The paper is organized as follows: Section 2 describes the methods, observational data, and numerical model formulation employed. Section 3 summarizes characteristics of the wind field near Barrow, reviews four generalized wind regimes and associated circulation states identified from the observational data, and extends the observational data with numerical model simulations. Limitations to the analyses and a summary of the results are presented in section 4.

2. Methods, Data, and Model Formulation

[6] During August–September 2005–2007, hydrographic surveys were conducted from the coastal research vessel, R/V Annika Marie, along a set of transects extending from the northern Alaskan coast across Barrow Canyon and across the Beaufort shelf (Figure 1). An Acrobat (Sea Sciences, Inc.) towed vehicle, equipped with a Seabird SBE 49 conductivity-temperature-depth (CTD), acquired high-resolution measurements of temperature and salinity along each transect in the upper water column (the shallower of, to within ∼3 m of the bottom or to ∼45–50-m depth) as the vessel motored offshore. Typical towing speeds were ∼3 m s^{-1} (∼6 knots), yielding water column

profiles every ∼0.15 km over the shelf and ∼1 km seaward of the shelf break. At the same time, an RDI 300 kHz downward-looking acoustic Doppler current profiler (ADCP) with bottom tracking was towed alongside the vessel to acquire water column profiles of current speed and direction to a depth of ∼100 m. The water column velocities were acquired at 1-m vertical resolution over the shelf and at 3-m vertical resolution off the shelf. Temporal averaging of the towed ADCP data resulted in ∼0.15 km horizontal spacing of the of water column velocities. Towed ADCP data were not acquired in 2005 owing to instrument failure.

[7] A Seabird 19plus CTD was used to acquire surface-to-bottom profiles of temperature and salinity to provide measurements in water depths greater than sampled by the Acrobat-borne CTD. Spacing between successive CTD casts ranged between ∼2 km and 12 km and, as such, only coarsely resolved horizontal hydrographic structure at off-shelf locations and depths for which there were not high-resolution data acquired by the Acrobat. These along-transect hydrographic (Acrobat and individual cast) data were interpolated to a regular 1-km horizontal by 1-m vertical grid from which geostrophic velocities were computed for the upper 60 m using the shallower of the bottom depth or 60 m as the level of no motion.

[8] A low-profile, bottom-mounted oceanographic mooring, instrumented with an upward-looking 300 kHz RDI ADCP was deployed about 17 km north of Cape Halkett (70° 58.875′N, 152° 15.039′W; ∼160 km east-southeast of Point Barrow) in 15 m of water on 16 August 2007 and recovered on 11 September 2007. The moored ADCP acquired water column velocity measurements in 0.5-m bins at 15-min intervals, but were subsampled at hourly intervals for comparison with hourly wind data.

[9] Wind speed and direction measurements at Barrow were obtained from the Atmospheric Radiation Measure-
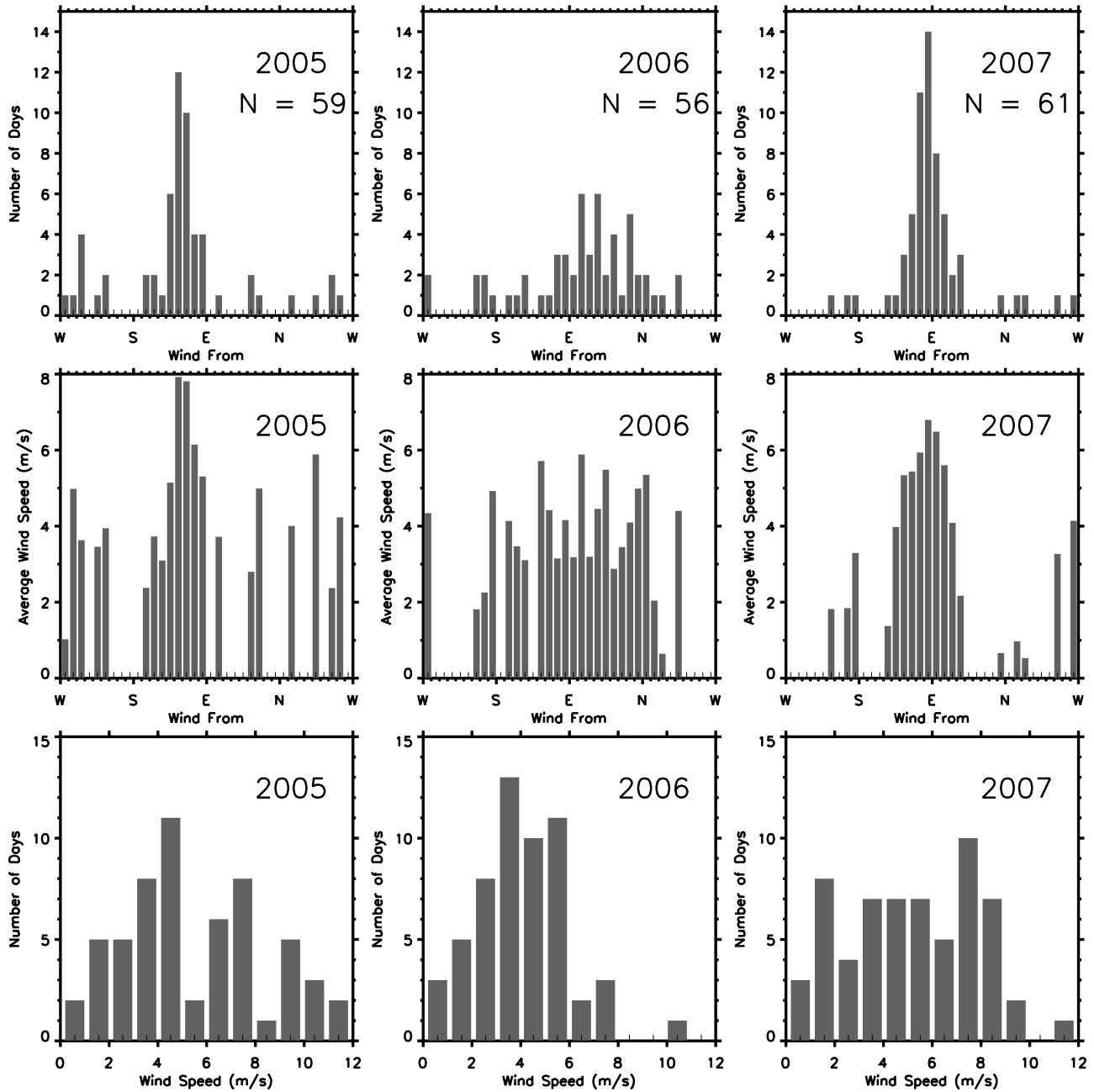
Figure 2. Summary of vector-averaged daily winds for August–September 2005–2007 at Barrow. (top) Histograms of vector-averaged daily wind direction, (middle) average wind speed as a function of wind direction, and (bottom) histograms of vector-averaged daily wind speeds.
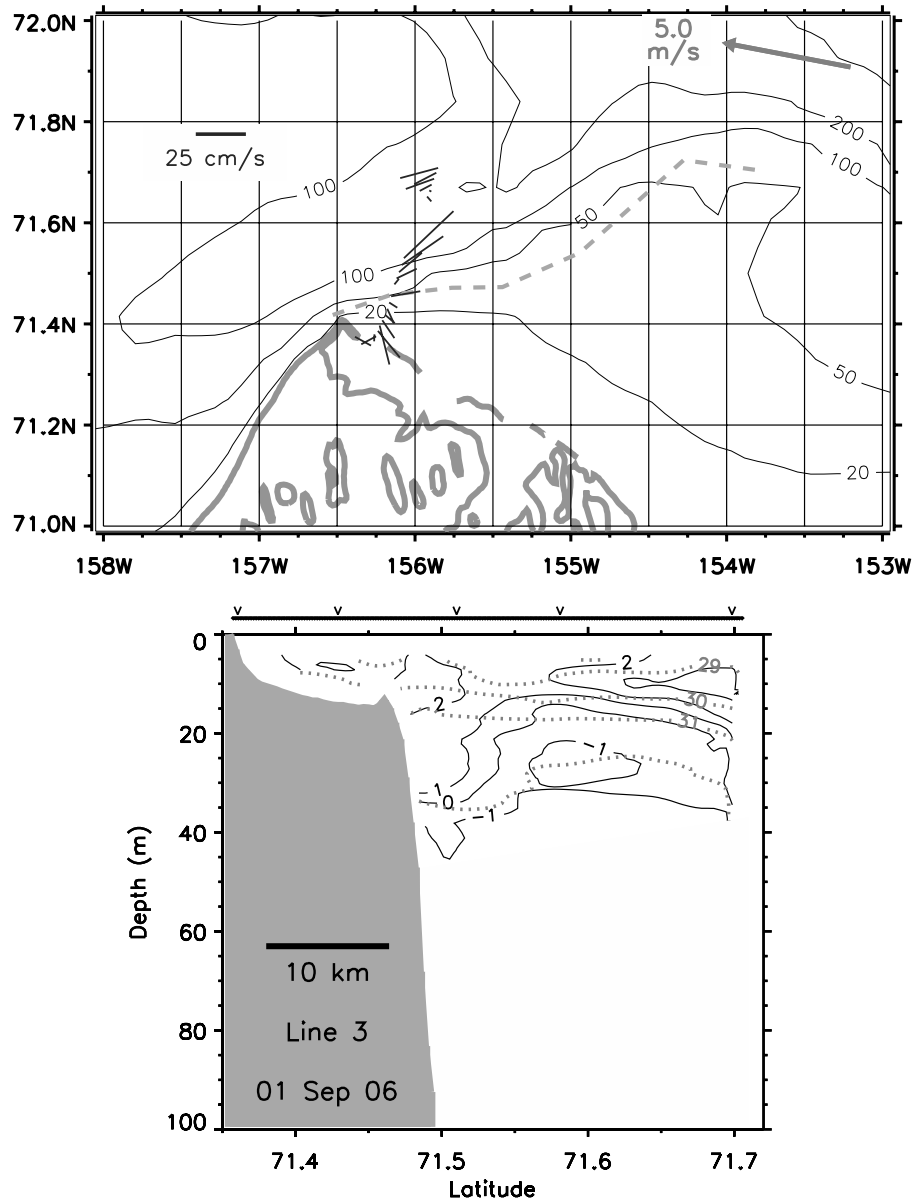
Figure 3a. Currents and water column temperatures and salinities observed along line 3 during winds from the east. (top) Paired plots of towed acoustic Doppler current profiler (ADCP) -measured surface (3–20 m averaged) current vectors, and (bottom) the cross section of the associated temperature/salinity fields. Isotherms are drawn as solid black contours and isohalines are drawn as dotted gray contours. Gaps in ADCP-measured currents occur where the bottom depth was greater than the depth range of the instrument (∼120 m). The annotated arrow in the top right corner of the ADCP vector plot indicates vector-averaged wind speed and direction for the 24-h period preceding and including that day's transect. The sinuous dashed line in the ADCP vector plot delineates the shelf break location identified from the hydrographic surveys. The horizontal lines across the top of the temperature cross sections identify the extent of towed Acrobat measurements, whereas the carets indicate locations of individual conductivity-temperature-depth (CTD) casts.
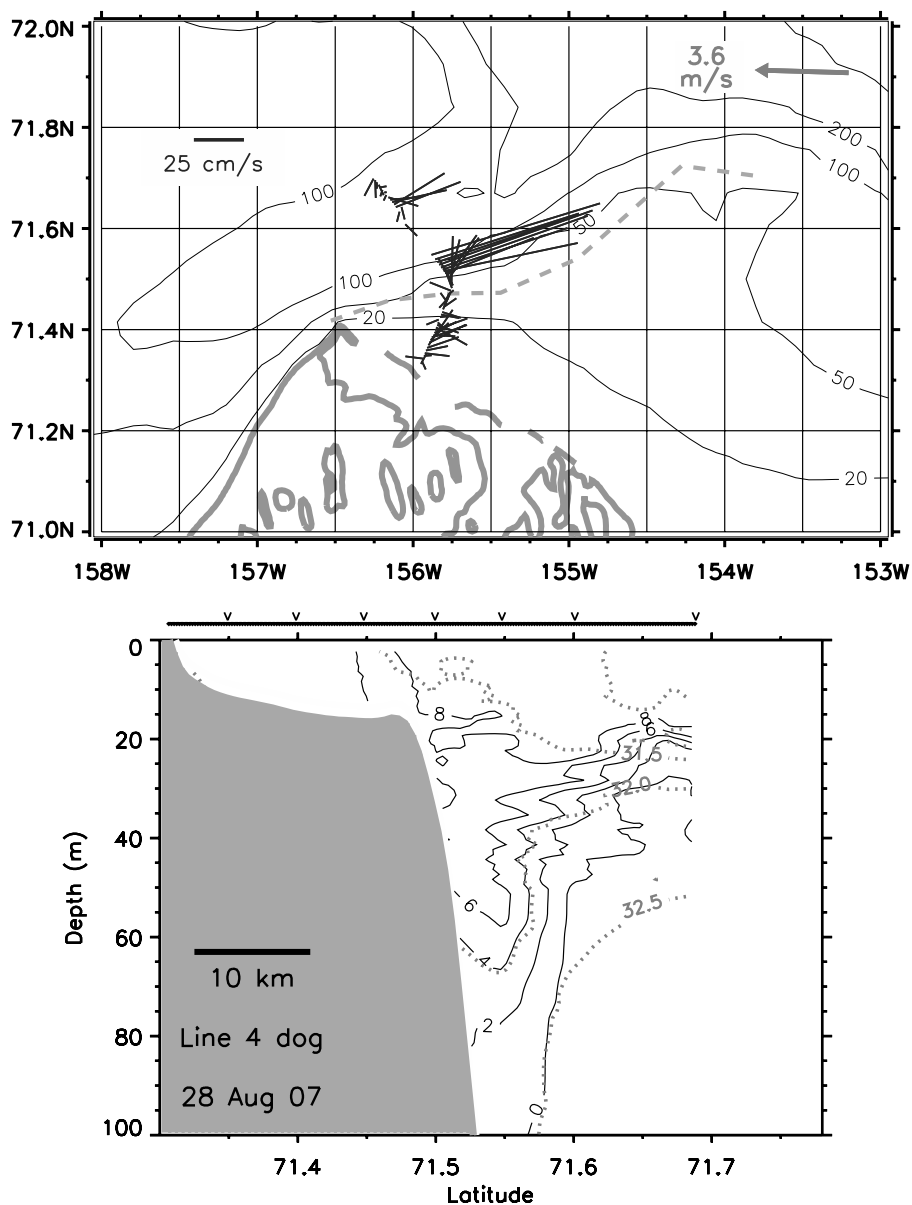
Figure 3b. Same as Figure 3a only for line 4 dogleg.

ment website (www.archive.arm.gov) for August and September of each field year. Hourly interval time series were generated for use as working data sets.

[10] Satellite sea surface temperature imagery from 2003 and 2007 was acquired to provide a broad spatial context for interpreting the field-based measurements described above. Level 0 Moderate Resolution Imaging Spectroradiometer (MODIS) Terra and Aqua data were retrieved from the NASA GSFC and were processed using SEADAS for sea surface temperature at 250-m resolution.

[11] The numerical model used is the pan-Arctic Naval Postgraduate School coupled sea ice-ocean model. This model has a horizontal grid spacing of 1/12° (or ~9 km) and 45 vertical depth layers with eight levels in the upper 50 m and fifteen levels in the upper 200 m. The model domain contains the sub-Arctic North Pacific and North Atlantic Oceans, the Arctic Ocean, the Canadian Arctic

Archipelago and the Nordic Seas (see Figure 1a of *Maslowski et al.* [2004] for model domain). Model bathymetry is derived from two sources: ETOPO5 at 5-min resolution for the region south of 64°N and International Bathymetric Chart of the Arctic Ocean (IBCAO) [*Jakobsson et al.*, 2000] at 2.5-km resolution for the region north of 64°N. The ocean model was initialized with climatological, three-dimensional temperature and salinity fields (Polar Science Center Hydrographic Climatology; PHC) [*Steele et al.*, 2000] and integrated for 48 years in a spin-up mode. The spin-up approach is especially important in establishing realistic ocean circulation representative of the time period at the beginning of the actual interannual integration. At the same time, the spin-up procedure was designed to force the model into a quasi-equilibrium state that is minimally sensitive to the specific initial conditions. The final run with realistic daily averaged European Centre for Medium-
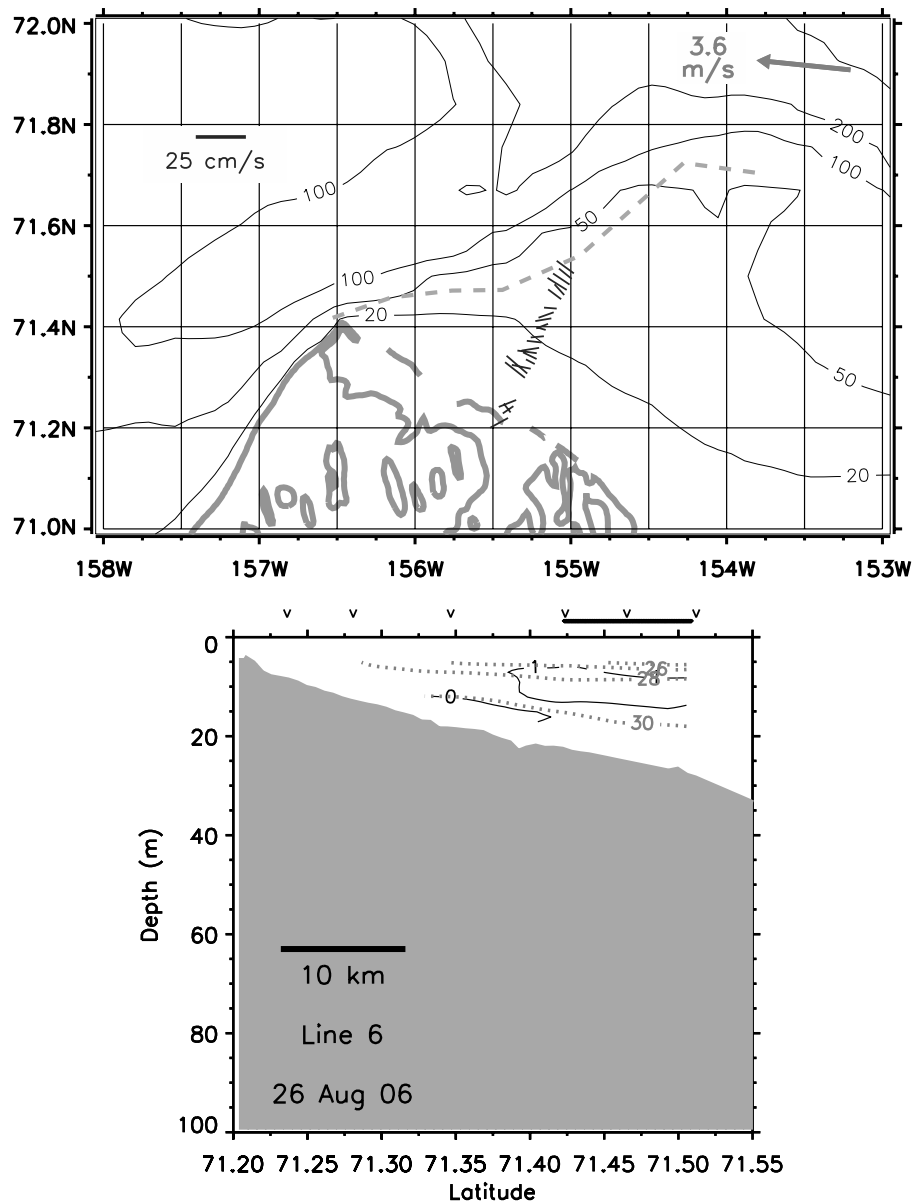
Figure 3c. Same as Figure 3a only for line 6.

Range Forecasts (ECMWF) interannual forcing starts in 1979 and continues through 2004. Results from this integration are used for the analyses in this paper. Additional details on the model including sea ice, river runoff, and restoring have been provided elsewhere [*Maslowski and Lipscomb*, 2003; *Maslowski et al.*, 2004]. We use two different archived model output products in this study; daily output and monthly mean output. Storage requirements for the full 26-year pan-Arctic three-dimensional suite of daily model output are prohibitive. Accordingly, only a small subset of the daily output is archived. Daily output from the surface layer (level 1) is archived. The next two layers for which daily output is archived are levels 5 and 10 (layer bottom depths are 26 m and 81 m, respectively). Because the inner Beaufort shelf in our study area is shallower than ~20 m, we use daily output only from the surface layer. The entire 26-year pan-Arctic three-dimensional record of

monthly mean model output is archived, however, and we present vertically averaged (layers 1–6; 0–33 m) monthly mean output as representative of near surface conditions.

3. Observations

3.1. Winds

[12] Daily vector-averaged winds at Barrow for August–September 2005–2007 are summarized in Figure 2. Figure 2 (top) shows that late summer winds were predominantly from the southeast in 2005, from the east-northeast in 2006, and from the east in 2007. Figure 2 (middle) shows that the highest wind speeds were generally associated with these prevailing winds. Figure 2 (bottom) shows the corresponding distributions of wind speeds. In this study, we characterize wind speeds less than 2 m s^{-1} as weak, wind speeds between
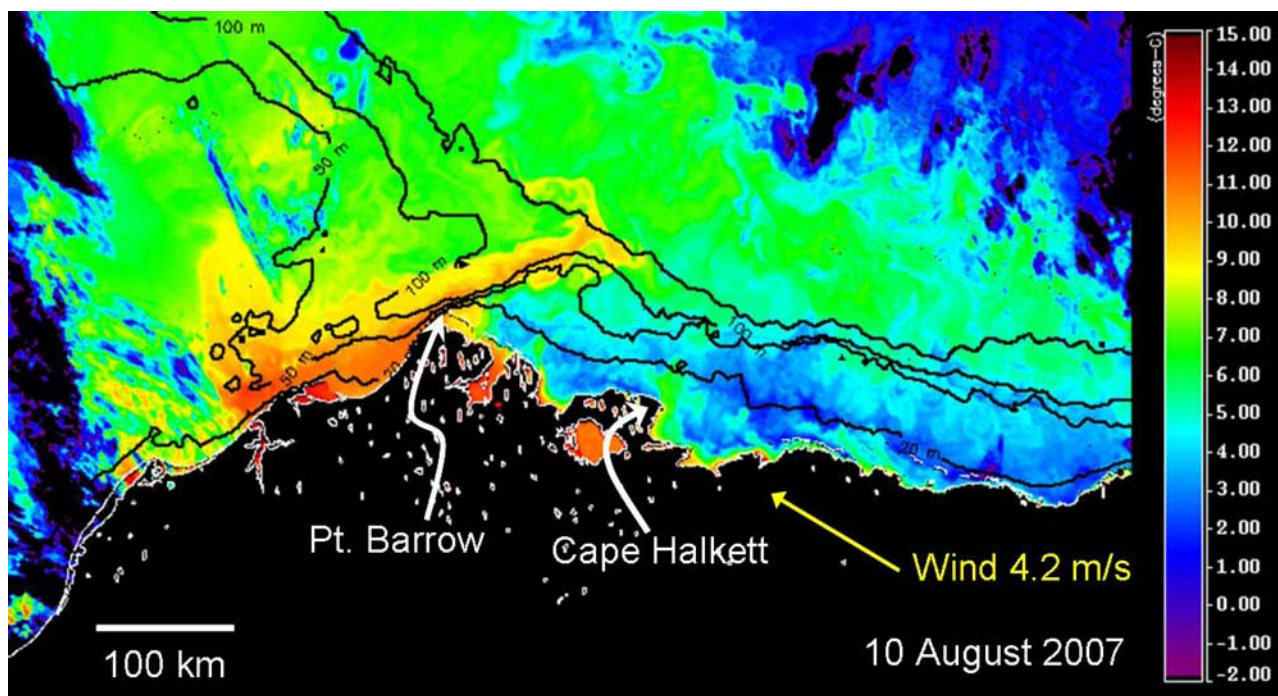
Figure 4. Moderate Resolution Imaging Spectroradiometer (MODIS) sea surface temperatures for 10 August 2007, 2335 UT.

2 m s^{-1} and 8 m s^{-1} as moderate, and wind speeds greater than 8 m s^{-1} as strong.

3.2. Currents During Winds From the East

[13] Figures 3 shows paired plots of ADCP-measured near-surface (vertical average of valid measurements acquired between 3 and 20 m) current vectors and corresponding temperature and salinity cross sections along transect lines occupied during moderate (~3.5–5.0 m s^{-1}) easterly winds. The line 3 (Figure 3a) and line 4 (Figure 3b) velocity stick plots and companion temperature cross sections indicate weak eastward intrusion of relatively warm Bering/Chukchi origin water onto the Beaufort shelf near Point Barrow despite the opposing winds, but northwestward flow across line 6 (Figure 3c) on the Beaufort shelf. Line 3 and line 4 temperature and salinity cross sections show isolines intersect the upper slope of Barrow Canyon indicative of baroclinic contributions to the ACC jet. The ACC velocity field, not well resolved except along line 4, depicts a strong northeastward flowing shelf break jet (~1 m s^{-1}) adjacent to the southern flank of Barrow Canyon.

[14] Figure 4 shows a MODIS sea surface temperature image acquired on 10 August 2007. Vector-averaged winds for the 24-h period preceding the image acquisition were from the east-southeast at 4.2 m s^{-1}. The image shows that warm Bering/Chukchi waters are carried northeastward by a well-defined ACC adjacent to the shelf break in Barrow Canyon in a manner consistent with that depicted in the line 4 velocity stick plot and temperature/salinity profiles (compare Figure 3b). The sea surface temperature (SST) image also shows a warm water intrusion onto the western Beaufort shelf near Point Barrow, the extent of which is similar to that suggested by the line 3 and line 4 velocity

stick plots and temperature plots. Temperatures over the majority of the Beaufort shelf are cooler (<5°C) than occur over the adjacent off shelf regions. On the basis of the line 6 velocity stick plot (Figure 3c), we infer that these cooler shelf waters are flowing along shore to the northwest. The absence of a well-defined southeastward flowing warm plume over the upper slope in the southern Beaufort Sea, downstream (east of) the mouth of Barrow Canyon suggests that the ACC jet has weakened within a relatively short distance from the canyon mouth. The absence of a strong ACC jet along the Beaufort shelf break is expected for these wind conditions because the Ekman response to east-southeasterly along-shore winds is sea level set down over the Beaufort shelf.

[15] As depicted in Figure 3 above, winds at Barrow in August–September 2005–2007 were predominantly from the eastern quadrant. The current meter data collected by the mooring at Cape Halkett and the Barrow wind data allow identification of the characteristic shelf flow associated with easterly winds and investigation of wind-forced changes to the characteristic current regime on the inner Beaufort shelf. Figure 5 shows the time series of vertically averaged U and V current components on the inner shelf near Cape Halkett and the concurrent winds at Barrow. Hourly time series of projected currents and winds are best correlated (R^2 = 0.75, current lags wind by 5 h) for a northwestward flowing (to 308°T) current driven by winds from the east-northeast (from 78°T). This wind-current relationship can be considered to be representative of late summer conditions. The best fit linear response of the projected current, C_p, to the projected wind, W_p, is

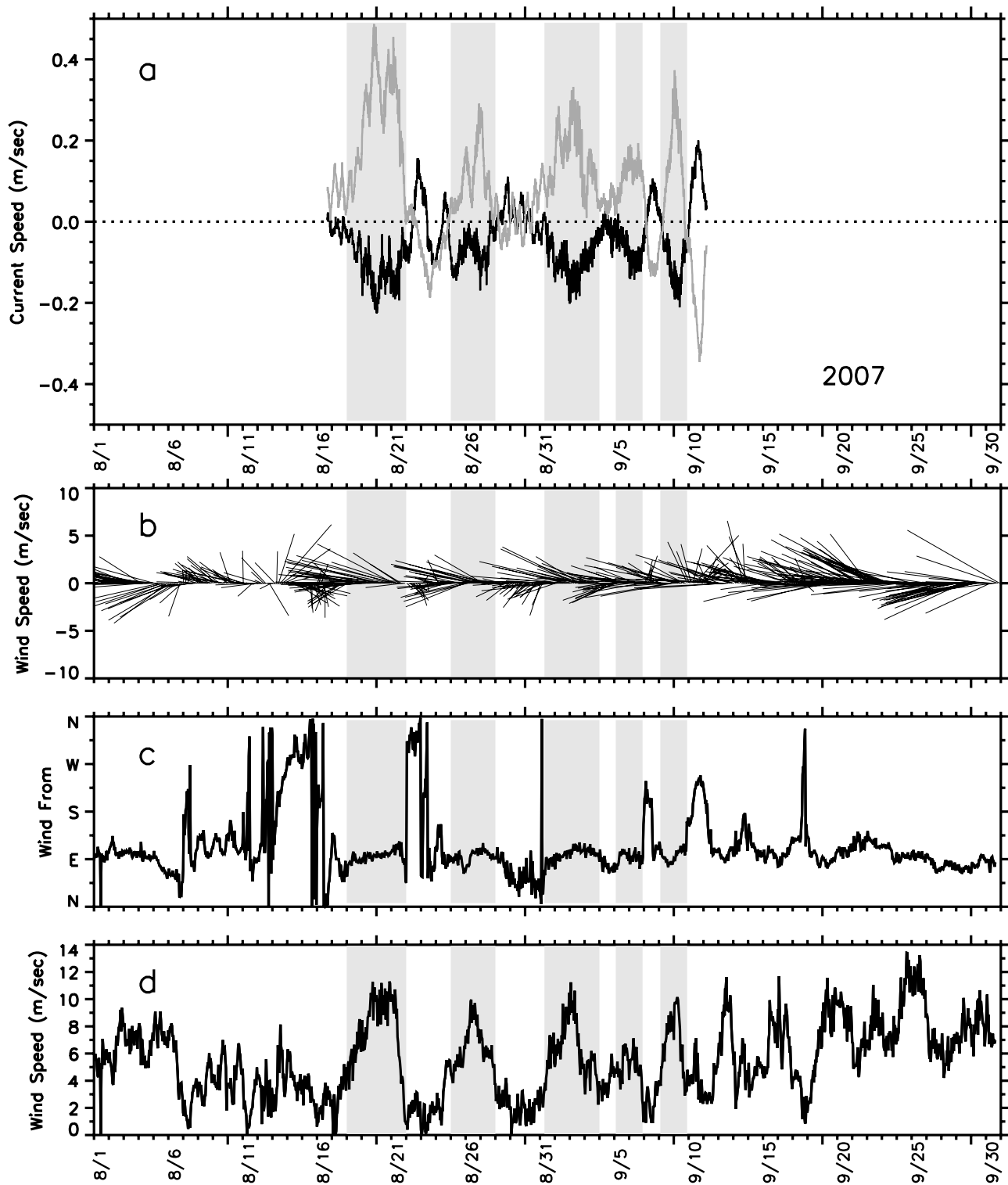$$C_p = 0.0687 + 0.0375 \cdot W_p \qquad (1)$$

Figure 5. (a) Time series of depth-averaged U (black) and V (gray) current components at Cape Halkett. Positive U and V velocities indicate eastward and northward flow, respectively. (b) Stick plot of winds at Barrow, (c) wind direction at Barrow, and (d) wind speed at Barrow. Grey shading is used to highlight northwestward flowing currents and concurrent winds.
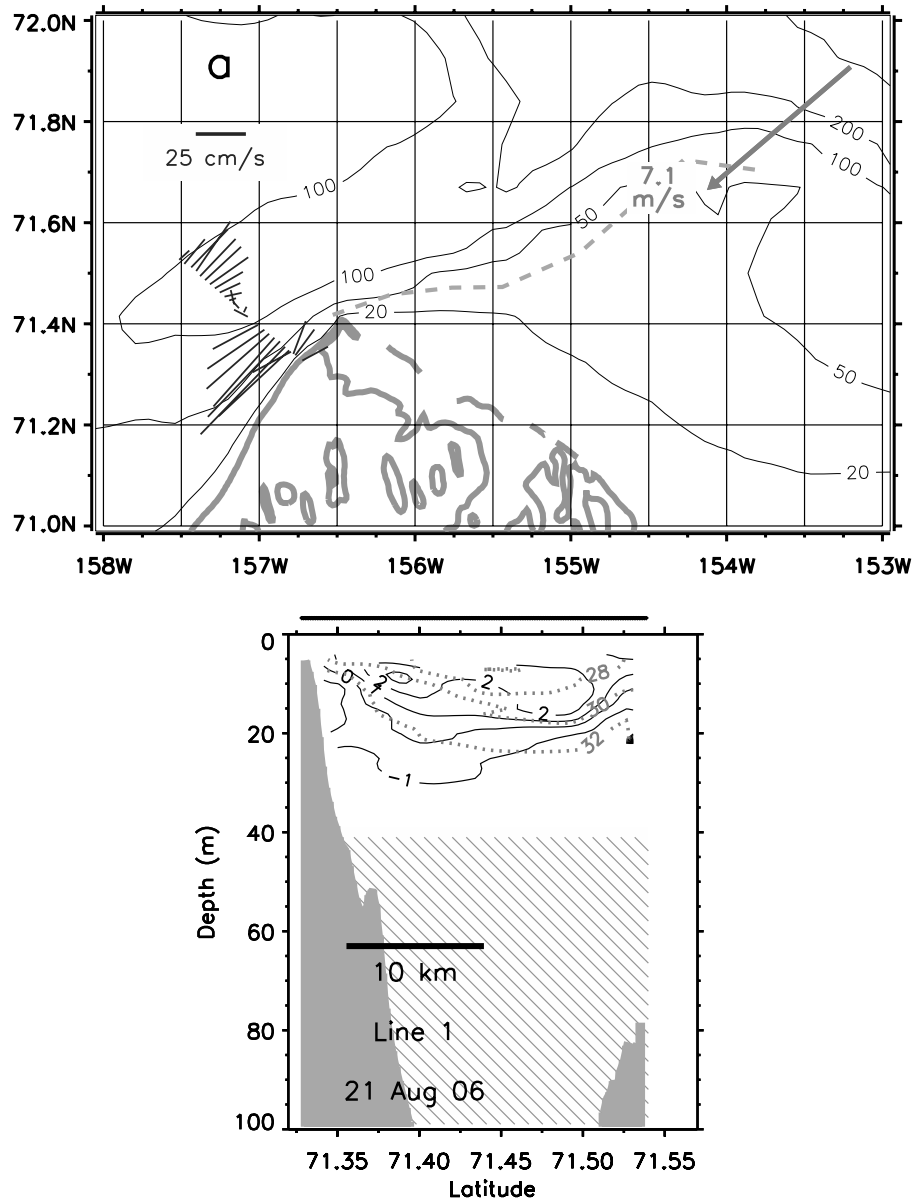
Figure 6. Currents and water column temperatures and salinities observed along line 1 during winds from the northeast. (top) Paired plots of towed ADCP-measured surface (3–20 m averaged) current vectors, and (bottom) the cross section of the associated temperature/salinity fields for lines (a) 1, (b) 2, (c) 3, (d) 4 dogleg, and (e) 5. Isotherms are drawn as solid black contours, and isohalines are drawn as dotted gray contours. Gaps in ADCP-measured currents occur where the bottom depth was greater than the depth range of the instrument (∼120 m). The annotated arrow in the top right corner of the ADCP vector plot indicates vector-averaged wind speed and direction for the 24-h period preceding and including that day's transect. The sinuous dashed line in the ADCP vector plot delineates the shelf break location identified from the hydrographic surveys. The horizontal lines across the top of the temperature cross sections identify the extent of towed Acrobat measurements, whereas the carets indicate locations of individual CTD casts.
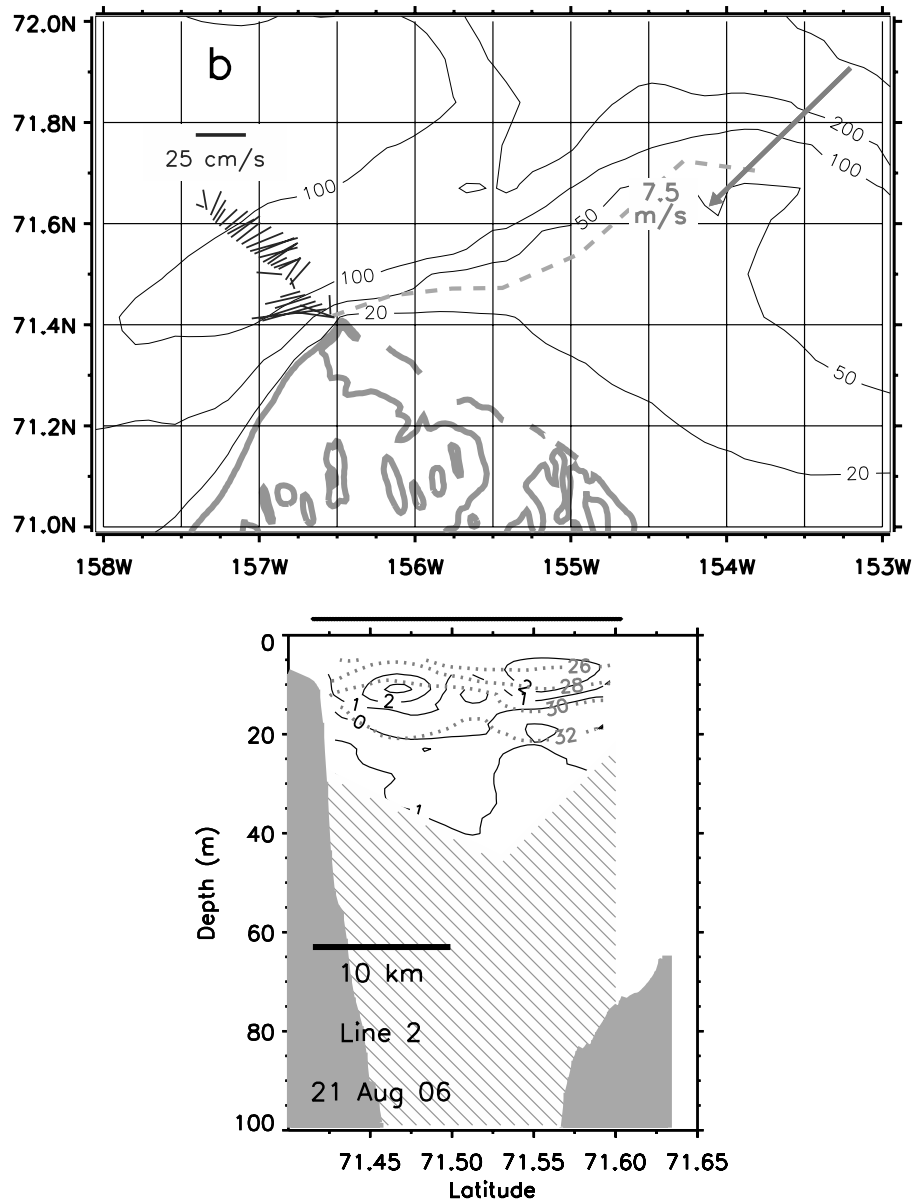
Figure 6. (continued)

in which a wind component from the east-northeast is negative and a wind component from the west-southwest is positive. Similarly, a positive value current is directed to the southeast and a negative value current is directed to the northwest. This relationship predicts that northwestward flow on the inner shelf reverses to the southeast when the east-northeasterly component wind speed falls below $1.8 \, \mathrm{m \, s^{-1}}$. Because winds at Barrow may not accurately reflect winds at Cape Halkett, the above statistical result should be considered to be semiquantitative. Nonetheless, this result along with the observations in Figures 3 and 4, indicate that northwestward flowing shelf waters driven by easterly winds inhibit significant eastward intrusion of warm Bering/Chukchi waters from Barrow Canyon onto the inner western Beaufort shelf.

3.3. Currents During Winds From the Northeast

[16] ADCP velocity stick plots (lines 1–5) show that moderate ($\sim$3.5–7.5 $\mathrm{m \, s^{-1}}$) northeasterly winds (upwelling favorable within Barrow Canyon) are sufficient to significantly alter the local circulation (Figure 6). The northeasterly winds promote sea level set down along the Chukchi coast, the result of which is to weaken and displace the ACC jet ($\sim$0.25–0.50 $\mathrm{m \, s^{-1}}$) away from the coast toward the northern side of Barrow Canyon thereby allowing northwestward flowing currents on the Beaufort shelf to turn southwestward at Point Barrow and flow up-canyon into the Chukchi Sea. Such flow reversals in Barrow Canyon have been reported by a number of authors [e.g., *Mountain et al.*, 1976; *Weingartner et al.*, 1998]. The twin temperature cores intersecting lines 1–5 in the upper $\sim$20 m, along with the counter current flows depicted in
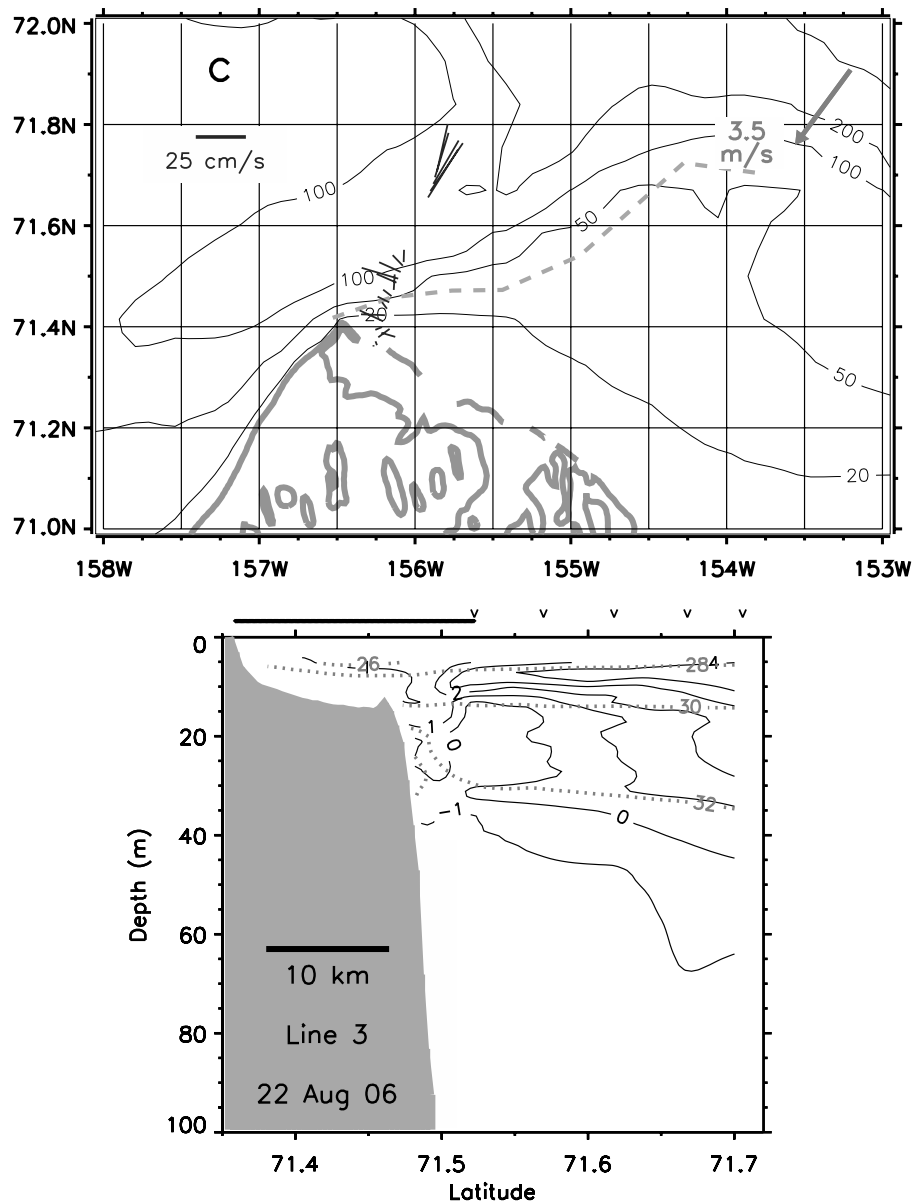
Figure 6. (continued)

the velocity stick plots for lines 1, 2, and 5 suggest that the warm core associated with the southwestward flowing currents represents, in part, a return branch of the displaced ACC. The temperature cross sections for lines 3 and 5 show the warmest waters were encountered well off shelf, near the outer ends of the respective section lines.

[17] Results from a barotropic numerical model study of wind driven circulation in the Chukchi and Beaufort Seas [*Winsor and Chapman*, 2004] are largely supported by the observations described above. Principal among these results were that east-northeasterly winds drive northwestward currents on the Beaufort shelf and reverse flow in Barrow Canyon.

3.4. Currents During Weak Wind Conditions

[18] Figure 7 shows paired plots of ADCP velocity stick plots (lines 2, dogleg 4, and 6), a geostrophic velocity plot

(line 8), and corresponding temperature/salinity cross sections along transect lines occupied during weak (<2 m s^{-1}) wind conditions. Collectively, these plots indicate that the circulation response to weak winds from any direction is a strong ACC jet (maximum speed $\sim$1 m s^{-1}) that follows the shelf break in Barrow Canyon and western Beaufort Sea and weak-to-moderate southeastward shelf currents carrying warm Bering/Chukchi origin waters well onto the outer shelf. An example of the spatial extent of a warm-water, on-shelf intrusion during weak wind conditions is illustrated by the 23 August 2007 MODIS sea surface temperature image (Figure 8). In this example, warm ($\sim$6$-$8°C) water has occupied the outer Beaufort shelf to $\sim$250 km east of Point Barrow.

3.5. Currents During Winds From the Southwest

[19] The MODIS SST image for 9 August 2003 (Figure 9) shows conditions during southwesterly winds following
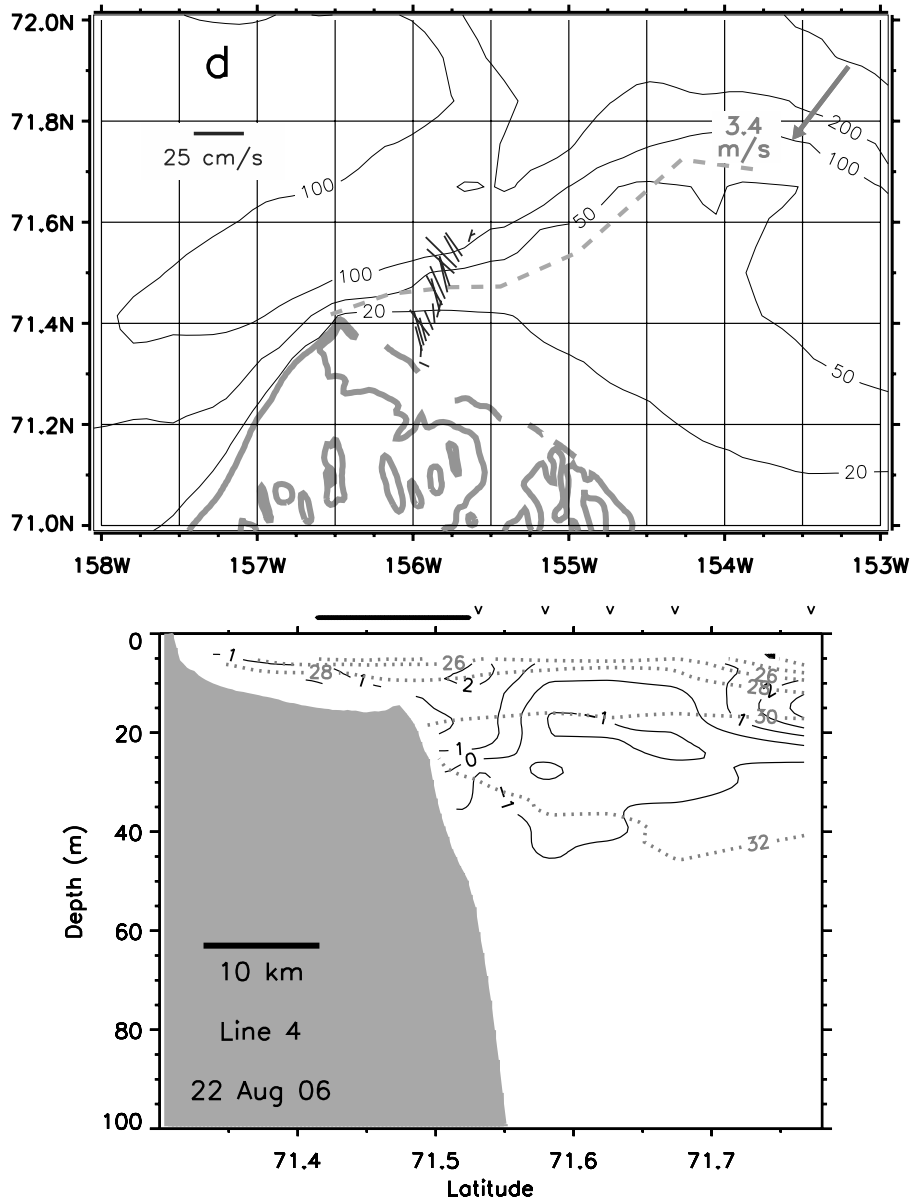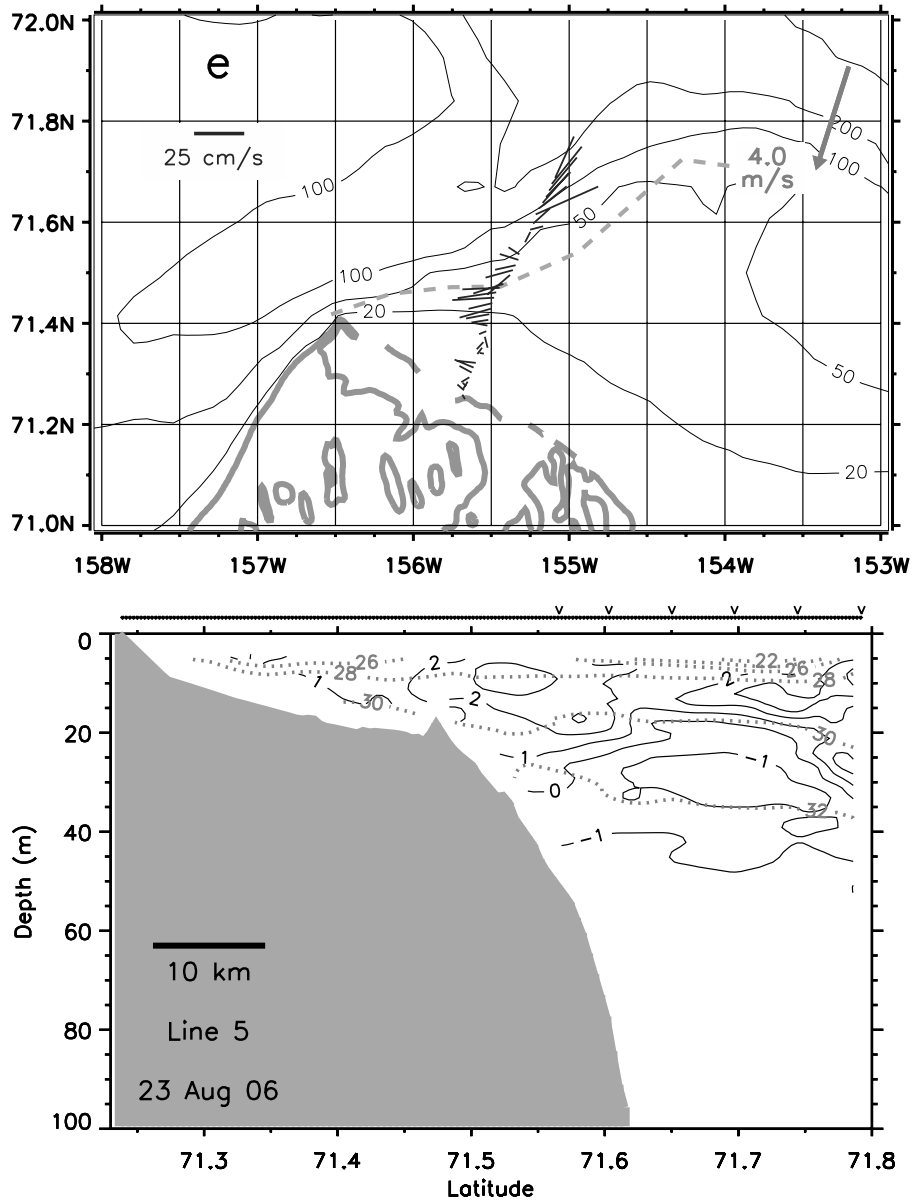
Figure 6. (continued)
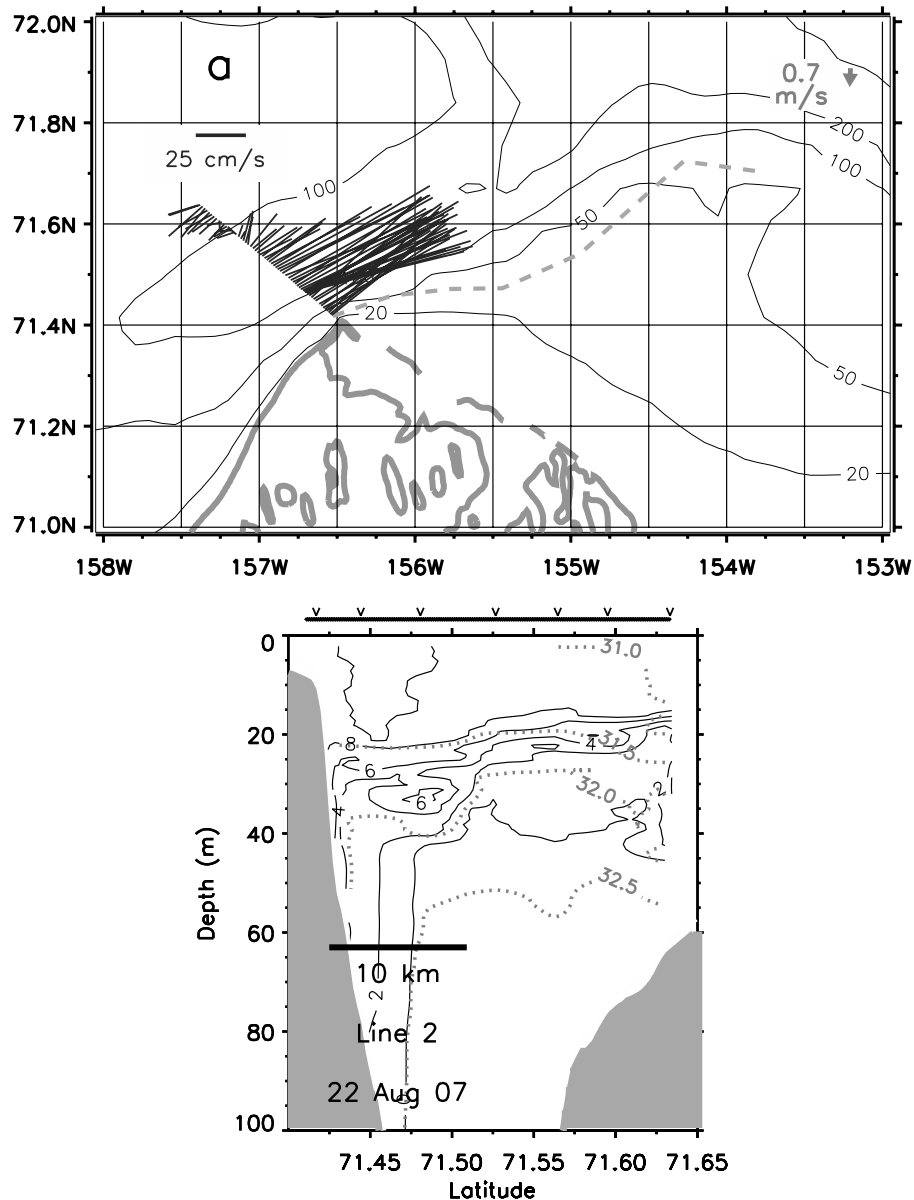
Figure 6. (continued)

Figure 7. Currents and water column temperatures observed during weak winds. (top) Paired plots of towed ADCP-measured surface (3–20 m averaged) current vectors, and (bottom) the cross sections of the associated temperature and salinity fields for lines (a) 2, (b) 4 dogleg, and (c) 6. Isotherms are drawn as solid black contours, and isohalines are drawn as dotted gray contours. The annotated arrow in the top right corner of the ADCP vector plot indicates vector-averaged wind speed and direction for the 24-h period preceding and including that day's transect. (d) The ADCP malfunctioned in 2005 so the top for line 8 depicts the baroclinic geostrophic velocity (east-southeastward flowing currents are drawn as dotted contours; west-northwestward flowing currents are drawn as solid contours; the contour interval is 5 cm s^{-1}). The level of no motion is 60 m and represents the maximum sampling depth of the Acrobat towed vehicle. The sinuous dashed line in the ADCP vector plot delineates the shelf break location identified from the hydrographic surveys. The horizontal lines across the top of the temperature cross sections identify the extent of towed Acrobat measurements, whereas the carets indicate locations of individual CTD casts.
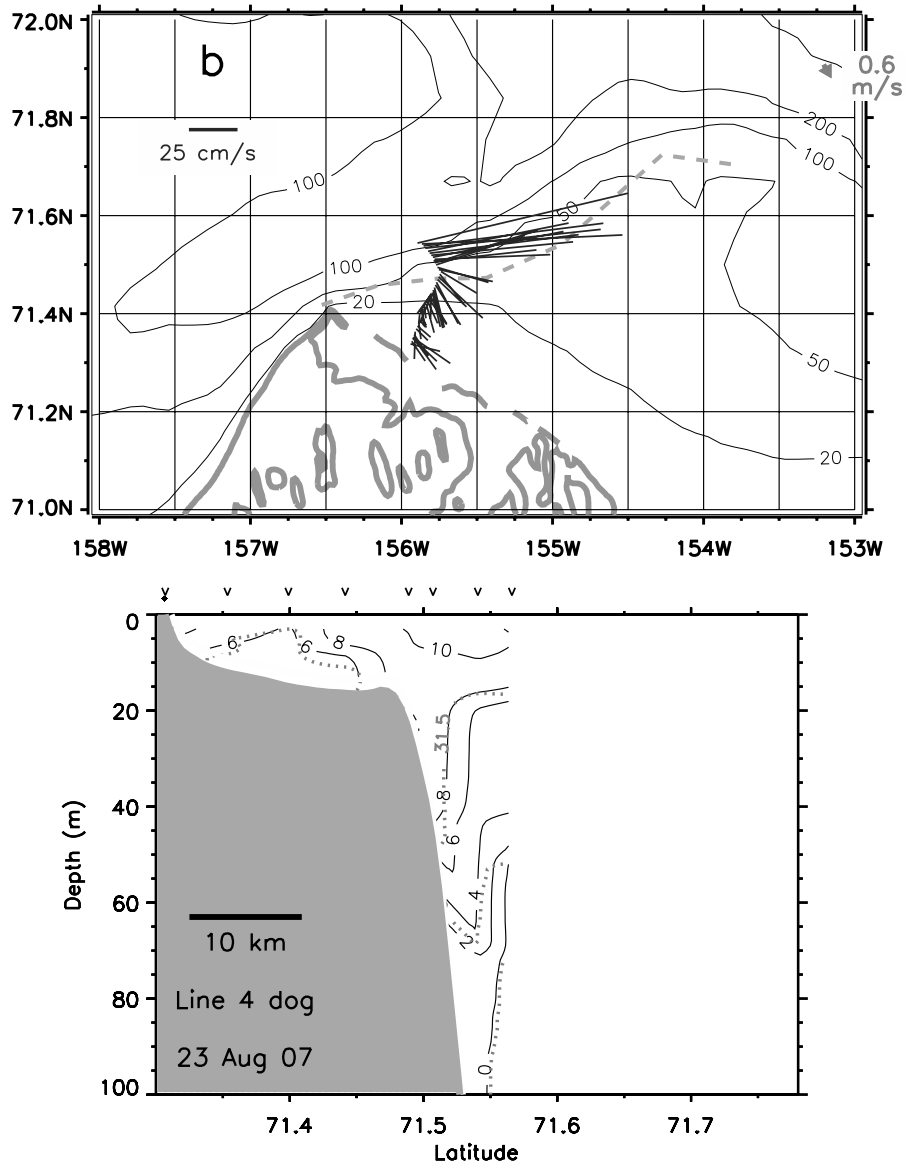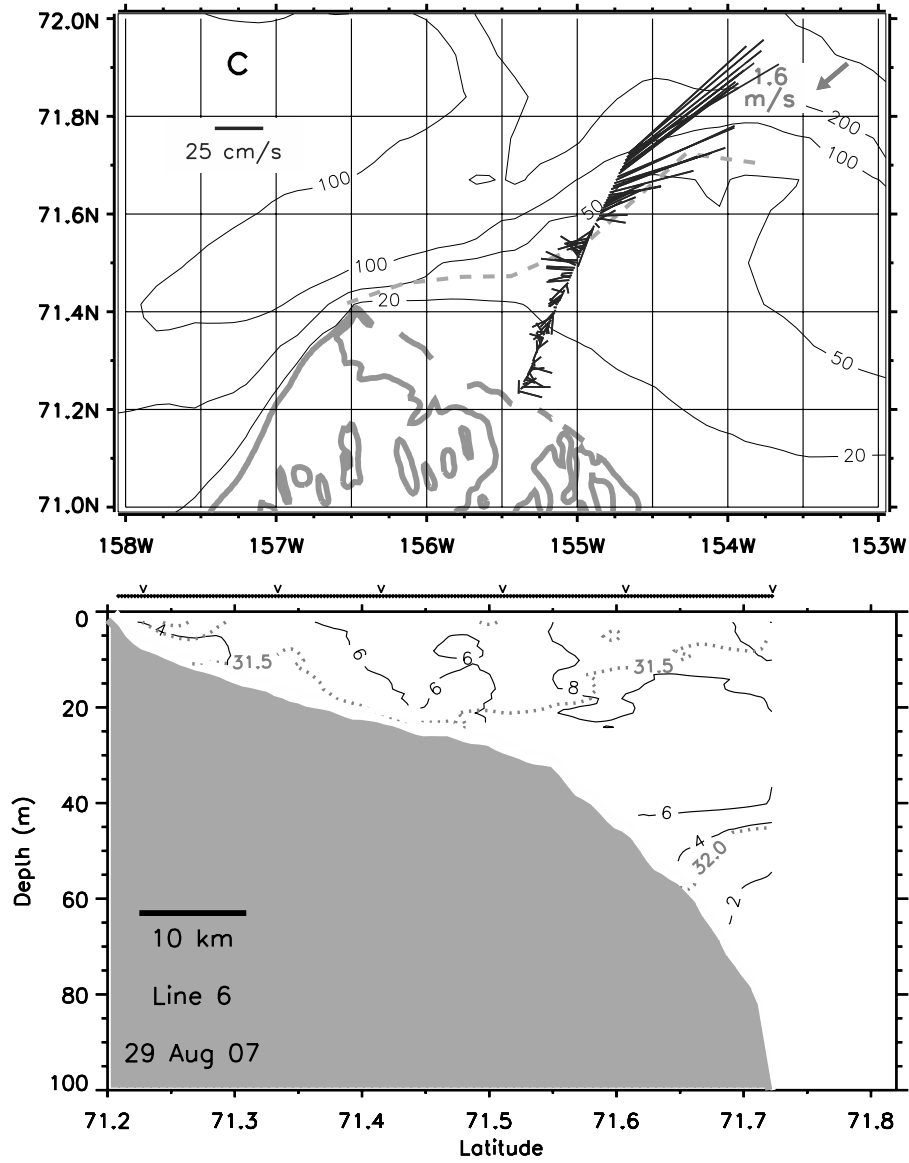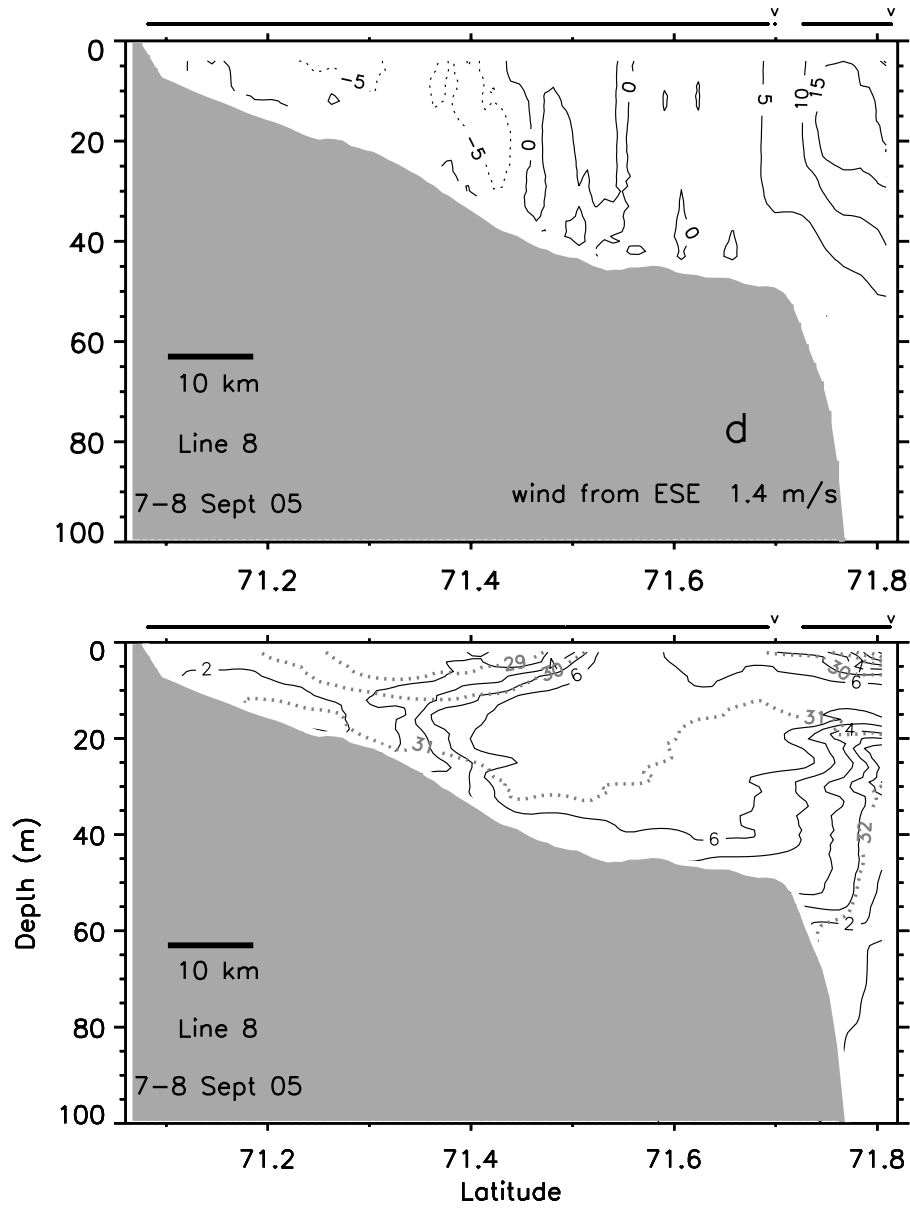
Figure 7. (continued)

Figure 7. (continued)

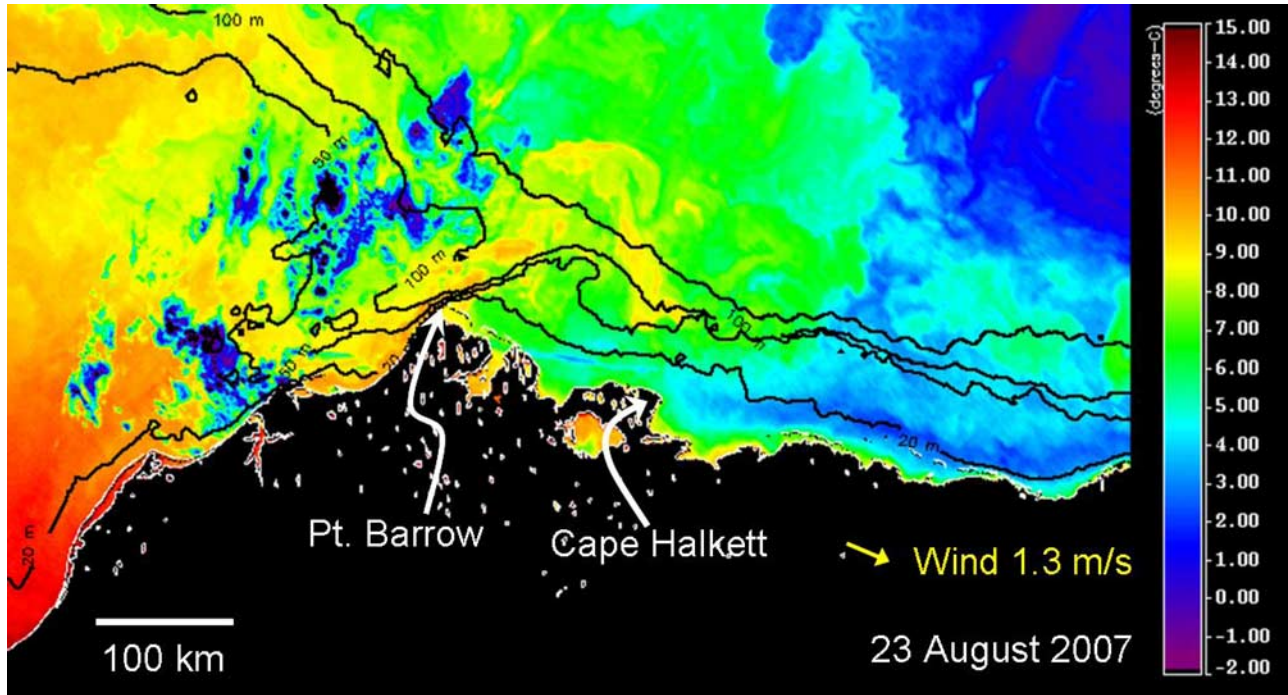**Figure 7.** (continued)

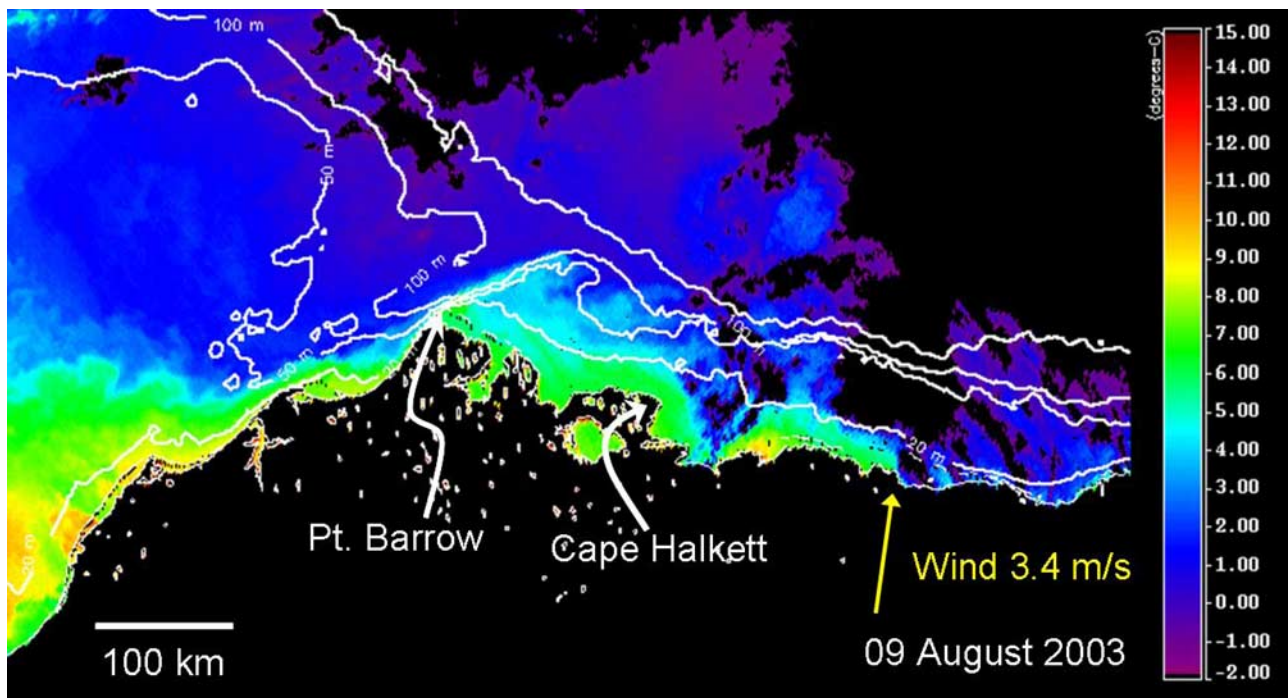**Figure 8.** MODIS sea surface temperatures for 23 August 2007, 2340 UT.

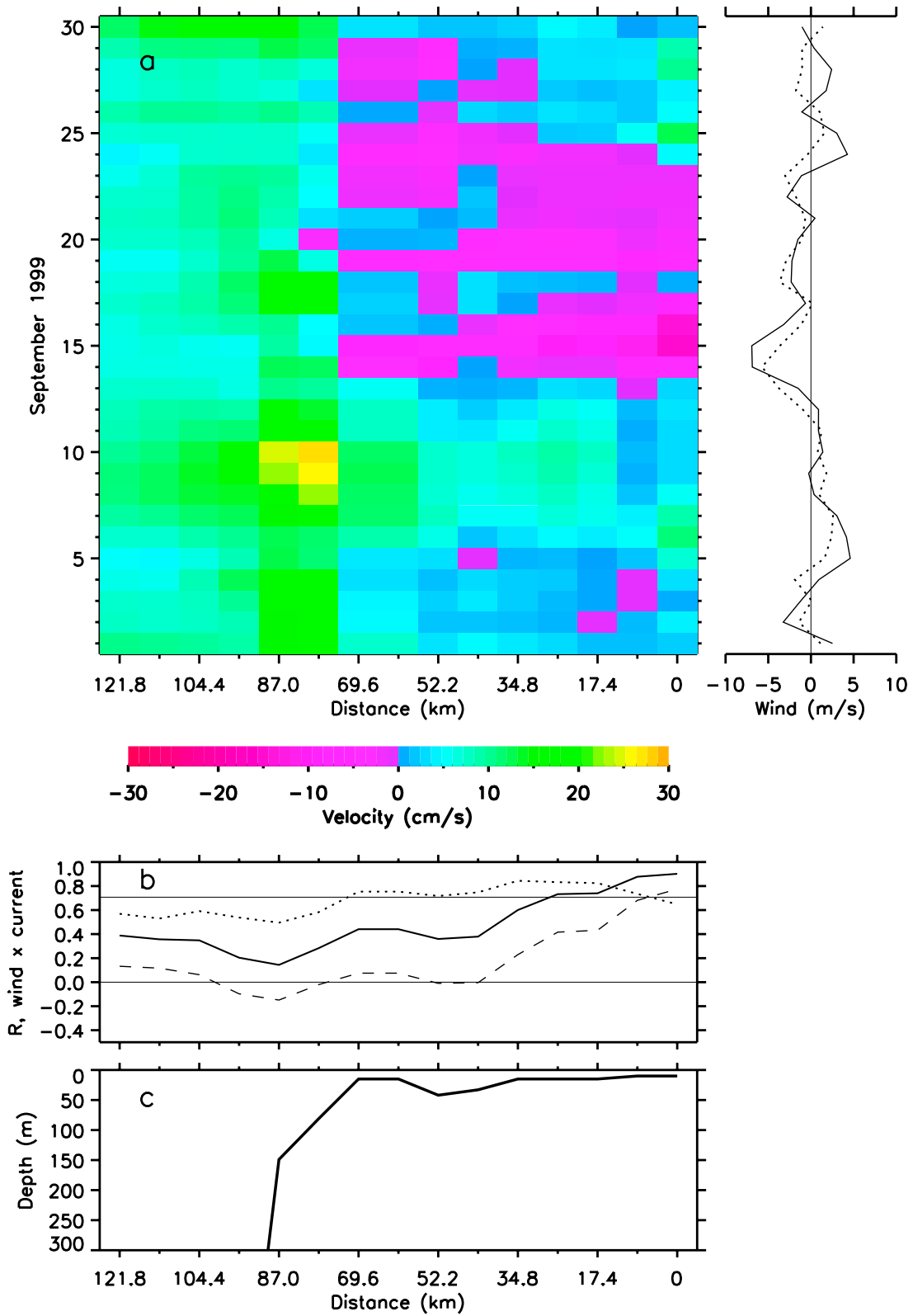**Figure 9.** MODIS sea surface temperatures for 9 August 2003, 0005 UT.

Figure 10

weeks of winds from predominantly the western quadrant. Winds from the southwest promote coastal convergence and sea level set up along the Alaskan Chukchi coast narrowing the distribution of warm water (6–8°C) in the Chukchi Sea to the vicinity of the coastline as Barrow is approached. The majority of the warm water turns to the southeast at Point Barrow intruding along the inner Beaufort shelf more 300 km east of Point Barrow. This coastal pathway differs from the outer shelf pathway followed during weak wind conditions (compare Figure 8).

3.6. Model Results

[20] High-resolution numerical circulation models can be useful tools to provide broader temporal and spatial contexts for interpreting limited observational data sets. Figure 10a shows a Hovmoller plot of daily surface current velocities normal to the West Shelf Line for September 1999. Daily model output from September 1999 is an arbitrary choice as there is no output for model years after 2004 to directly compare with 2005–2007 observations. Hovmoller plots of September daily output from other model years (not shown here) depict wind-current relationships similar to those described below.

[21] The corresponding time series of September daily projected ECMWF winds (E-W wind component is solid; NE-SW component is dotted) are shown to the right of the Hovmoller plot. Surface currents over the upper slope and outer shelf become stronger (>25 cm s^{-1}) when winds are weak or from the southwest. The surface expression of this shelf break jet appears to become poorly defined when winds are from the NE. Shelf currents flow to the east-southeast (max speed ~15 cm s^{-1}) when projected winds are from the W-SW. Flow over the shelf reverses to flow west-northwestward (~−15 cm s^{-1}) when the winds are from the E-NE. Close comparison of the daily currents depicted in the Hovmoller plot and the concurrent winds show that the currents lag the winds by about a day. The linear response of the surface currents to changes in the projected winds is summarized in the plot of coefficients for correlations between the time series of along-shore surface currents at each grid point and the time series of projected winds (Figure 10b). The correlation plot indicates that, over the entire shelf, more than 50% (R^2 > 0.5, current lags wind by 1 day) of the day-to-day changes in surface currents is explained by day-to-day changes in projected NE/SW winds. Correlations are weaker seaward of the shelf break.

[22] These relationships between winds and modeled daily currents are consistent with the observed relationships between winds and currents over the shelf and slope.

Monthly mean results are a convenient measure to present a multidecadal record of year-to-year changes in shelf currents and, by inference, intrusions of Bering/Chukchi origin waters onto the western Beaufort shelf.

[23] Figure 11a shows a Hovmoller plot of August–September averaged upper layer (surface to bottom or 33 m) model current velocities normal to the West Shelf Line for model years 1979–2004. The core of the ACC lies seaward of the shelf break and flows east-southeastward at velocities ranging from ~5 cm s^{-1} to 25 cm s^{-1}. Flow over the shelf is generally east-southeastward at speeds less than 10 cm s^{-1} with most of the few reversals occurring near the coast. The corresponding 1979–2004 time series of August–September averaged projected ECMWF winds (E-W wind component is solid; NE-SW component is dotted) are shown to the right of the Hovmoller plot. The linear response of the upper layer currents to changes in the projected winds is summarized in the plot of coefficients for correlations between the time series of along-shore currents at each grid point and the time series of projected winds (Figure 11b). The correlation plot indicates that, over the much of the shelf, more than 50% (R^2 > 0.5) of year-to-year changes in averaged summer currents is explained by year-to-year changes in the averaged local winds from the E/NE and W/SW octants. Variations in ACC velocities are less tightly coupled to changes in these local winds. This diminished response of the ACC is attributable, in part, to nonlocal forcing. Figure 11c shows the linear response of the upper layer heat transport across the west shelf line to the same projected winds. Year-to-year changes in heat transports are less well correlated with changes in the winds than are surface velocities. This relationship indicates that the heat content of the surface layer is influenced by processes other than advection driven by local winds. Because heat transport is itself a function of the current velocity field, the best correlations between wind and heat transport tend to occur at locations where the correlations between the current velocity field and the wind are elevated.

4. Discussion and Summary

[24] There are important limitations to the preceding analyses. Owing to the modest size of the vessel used, the safe acquisition of vessel-based hydrographic and towed ADCP current measurements was not possible in sea conditions associated with prolonged winds exceeding about 10 m s^{-1}. As a consequence, the vessel-based measurements reflect a bias toward more benign oceanographic conditions. The loss of bottom tracking by the

---

Figure 10. Naval Postgraduate School (NPS) coupled sea ice-ocean model results along the West Shelf Line. (a) Hovmoller plot of September 1999 daily surface velocities normal to the West Shelf Line. Positive (negative) velocities are directed to the E-SE (W-NW). Time series of September 1999 daily European Centre for Medium-Range Forecasts (ECMWF) projected winds are shown to the right of Hovmoller plot. Wind velocity component parallel to the E-W axis (solid line). Wind velocity component parallel to the NE-SW axis (dotted line). Winds to the E and to the NE are positive. (b) Coefficients for correlations between the time series of along-shore currents at each grid point and the time series of projected winds computed for currents lagging winds by 1 day (solid, E-W projected wind; dotted, NE-SW projected wind; dashed, SE-NW projected wind). A horizontal line corresponding to R = 0.707 (R^2 = 0.50) is included. (c) Depth profile along the West Shelf Line.
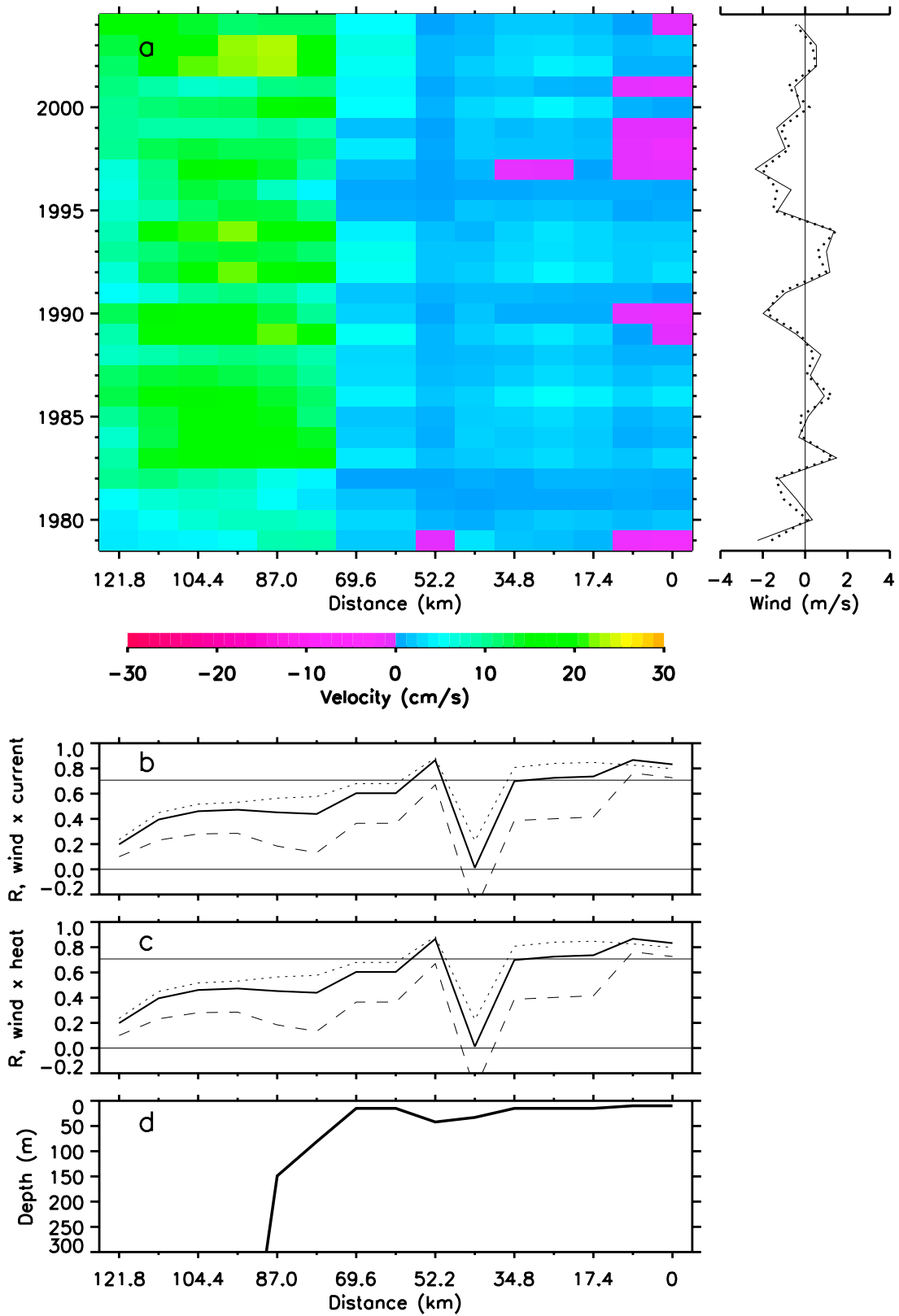
Figure 11

towed ADCP in water depths greater that ~120 m limited the off-slope extent to which the velocity structure of the ACC jet could be described to the shelf and the upper continental slope. Descriptions of changes to the current regime in Barrow Canyon were, therefore, not spatially comprehensive. Measurements of wind speed and direction at Barrow may not accurately reflect wind conditions elsewhere along the Alaskan north slope (e.g., at Cape Halkett). However, Figures 5, 10, and 11 suggests that Barrow winds are satisfactory for assessing qualitative wind-driven changes to currents on the Beaufort shelf within ~150 km of Point Barrow. Sea surface temperature imagery does not necessarily serve as a proxy for subsurface conditions and, in the absence of in situ measurements, inferred circulation should be viewed with some caution.

[25] Perhaps the most significant limitation to the model skill in simulating the regional circulation is that the ~9 km grid is not sufficiently fine to adequately resolve the ACC. The observations and analyses described above reflect late summer conditions. The distribution and concentration of sea ice will influence the transfer of wind energy to the ocean and may lead to current regimes that differ somewhat from those discussed herein. Finally, our descriptions of the wind-current relationships for the western Beaufort shelf are largely derived from observational (hydrography, currents, satellite imagery) snapshots acquired as components of projects whose focus was investigation of Bowhead whale feeding hot spots. Accordingly, a directed observational program to refine our understanding of the wind-current relationships in this region is likely warranted.

[26] In spite of these limitations, the in situ measurements, satellite observations, and model results described above permit some broad generalizations relating late summer wind forcing and the trajectory of (warm) Bering/Chukchi origin waters in the western Beaufort Sea to be drawn. When winds are moderate from the east or east-southeast, the ACC jet is relatively strong and flows adjacent to the shelf break along the southern flank of Barrow Canyon. These easterly winds drive inner shelf currents northwestward along the Beaufort shelf where they oppose significant eastward intrusions of warm water from Barrow Canyon onto the shelf. Because these easterly winds promote sea level set down over the Beaufort shelf and upwelling along the Beaufort slope, the ACC jet necessarily becomes weaker, broader, and displaced seaward from the Beaufort shelf break upon exiting Barrow Canyon (e.g., Figure 4). When winds are from the northeast, intrusion of warm waters onto the western Beaufort shelf does not appear to occur (compare Figure 6). However, moderate northeast winds cause separation of the ACC from the southern flank of Barrow Canyon and establish an up-canyon current along the southern flank that is fed in part by waters from the western Beaufort shelf. When winds are weak (compare Figures 5, 7, and 8) or from the southwestern quadrant (Figure 9), warm Bering/Chukchi waters are able to intrude onto the western Beaufort shelf.

[27] Comparison of Barrow winds and currents at Cape Halkett showed that inner shelf currents reversed to the southeast when the east-northeasterly component wind speed fell below 1.8 m s^{-1}. This threshold wind speed is essentially the same as that reported by *Hufford* [1973], who observed that eastward flow in opposition to the wind occurred on the Beaufort shelf when the wind speed fell below 2 m s^{-1}. A corollary to this observation is that any wind with a component from the west will promote intrusion of warm water onto the western Beaufort shelf.

[28] Daily output from the NPS model was shown to reasonably simulate the relationship between changes in winds from the eastern quadrant and the associated response of along-shore currents on the western Beaufort shelf (compare Figure 10). The Hovmoller plot of average August–September monthly mean model output (compare Figure 11) extends the observational data and daily model results to suggest that there is significant year-to-year variability in the amount of heat carried onto the Beaufort shelf. It can easily be inferred that changes in heat transported onto the historically under sampled western Beaufort shelf may influence both the timing and progression of sea ice melt in late spring-early summer as well as the timing and progression of sea ice formation in the fall.

Figure 11. NPS coupled sea ice-ocean model results along the West Shelf Line. (a) Hovmoller plot of August–September monthly mean, averaged upper layer (surface to shallower of bottom or 33 m) velocities normal to the West Shelf Line. Positive (negative) velocities are directed to the E-SE (W-NW). Time series of August–September averaged ECMWF projected winds are shown to the right of Hovmoller plot. Wind velocity component parallel to the E-W axis (solid line). Wind velocity component parallel to the NE-SW axis (dotted line). Winds to the E and to the NE are positive. (b) Coefficients for correlations between the time series of along-shore currents at each grid point and the time series of projected winds (solid, E-W projected wind; dotted, NE-SW projected wind; dashed, SE-NW projected wind). A horizontal line corresponding to R = 0.707 (R^2 = 0.50) is included. (c) Coefficients for correlations between the time series of heat transport at each grid point and the time series of projected winds (solid, E-W projected wind; dotted, NE-SW projected wind; dashed, SE-NW projected wind). A horizontal line corresponding to R = 0.707 (R^2 = 0.50) is included. (d) Depth profile along the West Shelf Line.

References

Aagaard, K. (1984), The Beaufort undercurrent, in *The Alaskan Beaufort Sea: Ecosystems and Environments*, edited by Peter W. Barnes et al., pp. 47–71, Academic, San Diego, Calif.

Ahlnas, K., and G. R. Garrison (1984), Satellite and oceanographic observations of the warm coastal current in the Chukchi Sea, *Arctic*, *37*, 244–254.

Hufford, G. L. (1973), Warm water advection in the southern Beaufort Sea August-September 1971, *J. Geophys. Res.*, *78*, 2702–2707, doi:10.1029/JC078i015p02702.

Jakobsson, M., N. Cherkis, J. Woodward, R. Macnab, and B. Coakley (2000), New grid of Arctic bathymetry aids scientists and mapmakers, *Eos Trans. AGU*, *81*(9), 89, doi:10.1029/00EO00059.

Maslowski, W., and W. H. Lipscomb (2003), High-resolution simulations of Arctic sea ice during 1979–1993, *Polar Res.*, *22*, 67–74, doi:10.1111/j.1751-8369.2003.tb00097.x.

Maslowski, W., D. Marble, W. Walczowski, U. Schauer, J. L. Clement, and A. J. Semtner (2004), On climatological mass, heat, and salt transports through the Barents Sea and Fram Strait from a pan-Arctic coupled ice-ocean model simulation, *J. Geophys. Res.*, *109*, C03032, doi:10.1029/2001JC001039.

Mountain, D. G., L. K. Coachman, and K. Aagard (1976), On the flow through Barrow Canyon, *J. Phys. Oceanogr.*, *6*, 461–470, doi:10.1175/1520-0485(1976)006<0461:OTFTBC>2.0.CO;2.

Paquette, R. G., and R. H. Bourke (1974), Observations on the coastal current of Arctic Alaska, *J. Mar. Res.*, *32*, 195–207.

Pickart, R. S. (2004), Shelf break circulation in the Alaskan Beaufort Sea: Mean structure and variability, *J. Geophys. Res.*, *109*, C04024, doi:10.1029/2003JC001912.

Shimada, K., T. Kamoshida, M. Itoh, S. Nishino, E. Carmack, F. McLaughlin, S. Zimmerman, and A. Proshutinsky (2006), Pacific Ocean inflow: Influence on catastrophic reduction of sea ice cover in the Arctic Ocean, *Geophys. Res. Lett.*, *33*, L08605, doi:10.1029/2005GL025624.

Steele, M., R. Morley, and W. Ermold (2000), PHC: A global ocean hydrography with a high quality Arctic Ocean, *J. Clim.*, *14*(9), 2079–2087.

Weingartner, T. J., D. J. Cavalieri, K. Aagaard, and Y. Sasaki (1998), Circulation, dense water formation, and outflow on the northeast Chukchi shelf, *J. Geophys. Res.*, *103*, 7647–7661, doi:10.1029/98JC00374.

Winsor, P., and D. C. Chapman (2004), Pathways of Pacific water across the Chukchi Sea: A numerical model study, *J. Geophys. Res.*, *109*, C03002, doi:10.1029/2003JC001962.

————————————

C. J. Ashjian, Department of Biology, Woods Hole Oceanographic Institution, Woods Hole, MA 02543, USA.

R. G. Campbell, Graduate School of Oceanography, University of Rhode Island, Narragansett, RI 02882, USA.

J. L. Clement-Kinney and W. Maslowski, Department of Oceanography, Naval Postgraduate School, Monterey, CA 93943, USA.

S. R. Okkonen and R. Potter, Institute of Marine Science, University of Alaska Fairbanks, Fairbanks, AK 99775, USA. (okkonen@alaska.net)